Journal of Aerosol Science 45 (2012) 50–57

Contents lists available at SciVerse ScienceDirect

Journal of Aerosol Science

journal homepage: www.elsevier.com/locate/jaerosci

Size distribution and chemical properties of welding fumes of inhalable particles

M. Oprya [a], S. Kiro [a], A. Worobiec [b], B. Horemans [b], L. Darchuk [b,*], V. Novakovic [b,c], A. Ennan [a], R. Van Grieken [b]

[a] Physico-Chemical Institute for the Environmental and Human Protection, National Academy of Science of Ukraine, Preobrazhenska 3, 65082 Odessa, Ukraine
[b] University of Antwerp, Department of Chemistry, Universiteitsplein 1, Wilrijk, Antwerpen 2610, Belgium
[c] Institute of Physics, Pregrevica 118, 11080 Belgrade, Serbia

ARTICLE INFO

Article history:
Received 20 April 2011
Received in revised form
12 October 2011
Accepted 14 October 2011
Available online 25 October 2011

Keywords:
Manual welding
Inhalable particles
Elemental composition
XRF analysis

ABSTRACT

The goal of the present study was to analyze the relationship between the fume formation rate, welding conditions, chemical composition of welding fume particles and their size. In the range from 0.25 to 16 μm aerodynamic diameter, three distinct types of welding fume particles were identified in the welder's breathing zone. The elemental composition of each type depended completely on the used welding materials, and reflects their mechanism of formation. Their relative abundance in the welding fume appeared to be dependent on the electrode coating, as well as the heat input during welding.

1. Introduction

It is well known that the processes of arc welding through fusion are accompanied by the formation of aero-disperse toxic particles (0.005–20 μm), commonly referred as 'welding fume' (WF). The current methodology for assessing harmful effects of WF particles on both the welder's health and the environment is based on the definition of toxicity (dose-effect) for some WF components, and their concentration in the workshop area (International Standards Organization, 2002). In other words, the assessment is based on the comparison between the amount of toxic components in the WF and their corresponding maximum limit values. However, this method does not take into account the variety of sizes, shapes and chemical compositions of WF particles according to other authors' results (Jenkins et al., 2005; Sowards et al., 2008; Voitkevich, 1995; Worobiec et al., 2007; Zimmer & Biswas, 2001). These features are important from a toxicological perspective, because the penetration and precipitation efficiency of WF particles into the human respiratory tract depends strongly on the particle size (Hewett, 1995). In addition, the physical and chemical properties as well as the biological effects of ultra-fine WF particles and their aggregates can differ strongly from characteristics of WF macroscopic dispersions. For example, the increased chemical potential at the high curvature interface of ultra-fine particles and the large specific surface of aggregates could drastically change the solubility, sorption capacity, reactivity and catalytic ability

* Corresponding author.
E-mail address: larysa.darchuk@ua.ac.be (L. Darchuk).

(Holsapple et al., 2005). A study on the chemical composition of size segregated WF particles is therefore of great importance.

WF particles are usually classified into three types according to the mechanism of their formation (Jenkins et al., 2005; Sowards et al., 2008; Zimmer & Biswas, 2001): (1) ultra-fine particles (less than 0.1 μm) formed by condensation from the gas phase, saturated with substances from both the electrode and weld metal; (2) coarse fume particles (larger than 1 μm) formed by mechanical means such as ejection of microscopic electrode material droplets (microspatter) from the arc or molten weld pool; and (3) particles (agglomerates of various shapes and densities) larger than 0.1–0.2 μm, which are mainly formed by coagulation of ultra-fine particles. It is usually assumed that the size of agglomerates does not exceed 2–3 μm (Jenkins et al., 2005; Voitkevich, 1995; Zimmer & Biswas, 2001). When shielded metal arc welding (SMAW) is applied, the latter two types of particles mostly prevail (98–99% of WF mass) in the welder's breathing zone (Sowards et al., 2008). Most of the WF ultra-fine particles formed during SMAW consist of a core containing iron and manganese compounds (Fe_3O_4 and $MnFeO_2$) and a shell rich in silicon, calcium, potassium, sodium and fluorine (depending on the composition of the electrode coating) (Voitkevich, 1995). The chemical composition of coarse WF particles differs strongly from that of ultra-fine particles. They contain mostly iron and slag melt components (Worobiec et al., 2007). Additionally gases formed during welding processes (e.g. CO_2, HF, and SiF_4) could be adsorbed on the particle surface, or could be trapped by the agglomerates. The local concentration of the adsorbed gases could exceed their total content in the gas phase (Voitkevich, 1982).

The above described heterogeneous structure and multi-element composition of WF particles make them different from other industrial aerosols. Furthermore, these features make it difficult to evaluate the environmental and health effects of WF particles, and they do not allow the objective comparative hygienic evaluation of different types of welding materials. Therefore, chemical composition and particle size are both equally important factors to be considered for characterizing of the WF.

Two approaches on the elemental analysis of size segregated WF particles are described and compared in this paper: (1) determination of the bulk chemical composition of inhalable WF fractions and (2) analysis of the chemical composition of individual WF particles.

2. Experimental

Mild steel plates have been chosen for automated single-pass surfacing (surface) welding. The 4 mm diameter commercial electrodes covered by rutile (TiO_2) (Paton ANO-4 electrode, American Welding Society classification E6012), ilmenite ($(Fe,Mn)TiO_3$) (Paton ANO-4i electrode) and carbonate–fluorite ($CaCO_3$–CaF_2) (Paton UONI 13/45, AWS classification E6015) have been used for SMAW. The wire was the same for all used electrodes.

Surfacing welding in the form of welding bead was applied, since it provides a maximum WF formation rate. Welding was performed in a specially designed chamber (Worobiec et al., 2007) under conditions of positive current, reverse polarity, and a welding speed of 300 mm min^{-1}. Two arc energy heat input levels were applied for SMAW: 1.0 ± 0.1 kJ mm^{-1} (180 A, 28 V) and 1.36 ± 0.15 kJ mm^{-1} (210 A, 32 V).

In order to obtain representative samples of welding aerosols, the generated WF was collected by extracting the air at a distance of 0.4 m to the welding arc with a flow of 75 l s^{-1}. It was redirected into a vertical pipe with a diameter of 0.19 m and a length of 1.2 m. The air flow profile inside the pipe was carefully determined with an anemometer in order to identify equivalent sample collection spots. The air flow rate at the sampling spots was 2.7 ± 0.2 m s^{-1}, and the concentration of the collected WF particles ranged from 110 to 210 mg m^{-3} depending on the welding parameters and type of electrode. The experimental design allowed the simultaneous collection of up to four independent WF samples (see Fig. 1). The sampling points were equipped with specially designed nozzles for isokinetic collection of the WF particles, depending on the flow characteristics of the impactor.

Bulk samples of WF fractions were collected with Harvard-type single-stage low-pressure impactors (Air Diagnostic and Engineering Inc., Harrison, ME, USA) (Lioy et al., 1988; Marple et al., 1987). Three distinct types were used, each with a sharp 50% cut-off efficiency for particles with an equivalent aerodynamic diameter (EAD) of 1, 2.5, and 10 μm (at an air-flow of 23, 10, and 10 l min^{-1}, respectively). The particle impaction plates were covered with white mineral oil (Sigma-Aldrich) to avoid particle bounce and blow-off. The resultant welding fume fractions, i.e. EAD ranging from 0 to 1 μm (PM_1), 0 to 2.5 μm ($PM_{2.5}$) and 0 to 10 μm (PM_{10}), were homogeneously collected for about 10 ± 1 s on ring supported Teflon membrane filters (TK15-G3M 37 mm, Pall, Ann Arbor, MI, USA). Before and after collection, filters were conditioned for minimum 48 h in a clean and climate controlled room ($T = 20 \pm 1$ °C, RH $= 50 \pm 5$%), followed by gravimetrical analysis on a MX5 microbalance (accuracy: 1 μg, Mettler Toledo, Columbus, OH, USA). The bulk WF samples were analyzed with X-ray fluorescence (XRF) spectrometry in order to determine their elemental composition. Concentrations (μg $filter^{-1}$) for 20 elements (Al, Si, S, Cl, K, Ca, Ti, V, Cr, Mn, Fe, Ni, Cu, Zn, As, Se, Sr, Cd, Sb, Pb) were determined on a high-energy polarized-beam energy-dispersive XRF spectrometer (Epsilon-5, PANalytical, Almelo, The Netherlands) according to the procedure described by Spolnik et al. (2005). As, Se, Cd, and Sb were not detected in any of the samples and were not considered in further discussions. The obtained bulk elemental concentrations allow to study the chemical composition of WF particulate matter in fractions with a different penetration efficiency in the human lungs (Hewett, 1995).

Size-segregated WF aerosol samples were collected by a Berner cascade impactor (LPI 0.06/30 l min^{-1}). The cut-off diameters of the used impactor stages were 0.0625, 0.125, 0.25, 0.5, 1.0, 2.0, 4.0, and 8.0 μm EAD. In order to analyze the

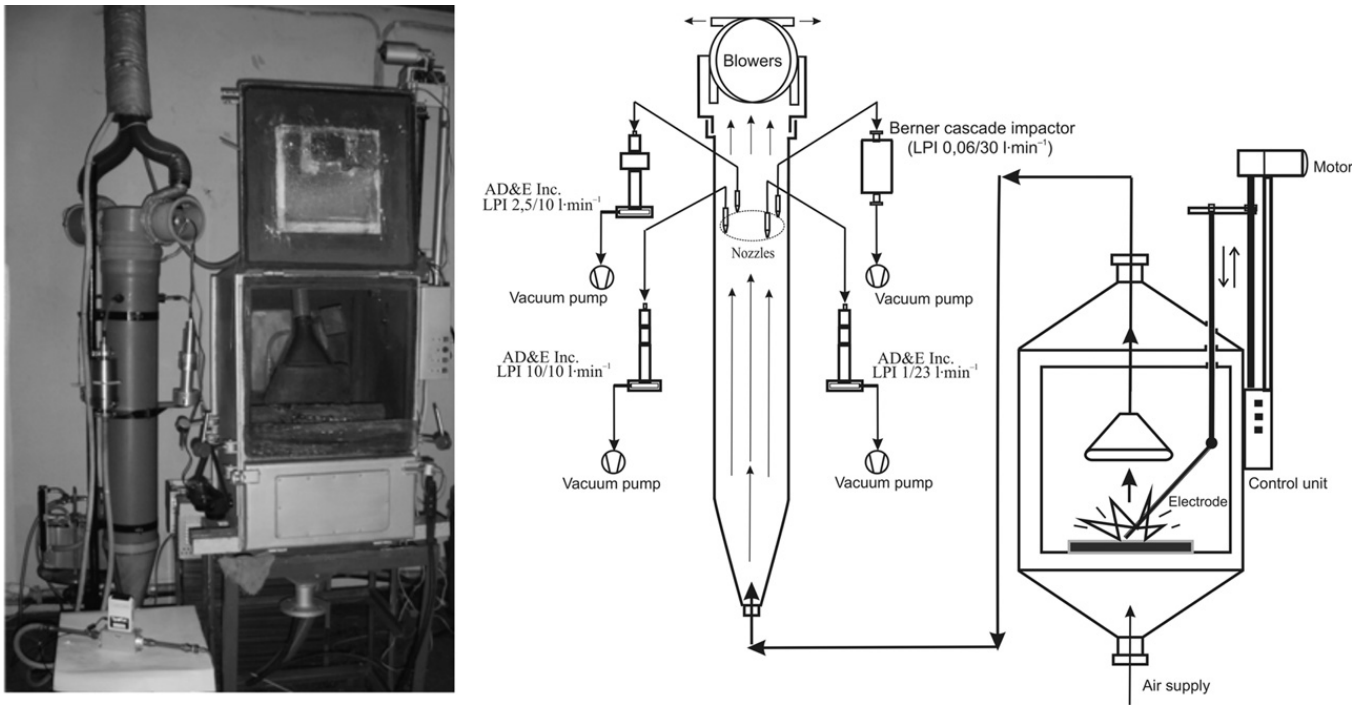

Fig. 1. Welding and fume collection equipment.

total mass of WF particles in each of these fractions, samples were collected on cellulose filters for about 70 s. The determination of their weights was fulfilled as described for bulk WF particle fractions. Separate samples for analyzing the elemental composition of individual WF particles were collected on the upper 6 stages of the Berner impactor. Si wafers were used as a substrate for the collection of the finest particulate fractions (cut-off diameters of 0.25 and 0.5 μm EAD), while the particles with cut-off diameters of 1, 2, 4, and 8 μm EAD were deposited on Ag foils, in accordance with the recommendations (Szalóki et al., 2001). A sampling time of 5 s was applied for fractions 0.25 and 0.5 μm EAD, while a total collection time of 30–70 s was found to give optimal loadings for fractions 1, 2, 4, and 8 μm EAD. The elemental composition of the individual WP particles was obtained by JEOL 733 electron-probe microanalysis (EPMA) device, equipped with a super-atmospheric thin window OXFORD energy-dispersive X-ray detector, which is especially suited for low-Z elemental analysis (starting from C). About 100 particles per sample were analyzed manually for stages 3 and 4 of the Berner impactor. The analysis of about 300 particles per sample was automated for stages 5, 6, 7, and 8. More information on the instrument and analytical procedure could be found elsewhere (Worobiec et al., 2007; Ro et al., 1999). The X-ray spectra of the individual particles were evaluated by non-linear least-squares fitting, using the AXIL code (Vekemans et al., 1994) and the semi-quantitative elemental composition was calculated with an iterative approximation method based on Monte Carlo simulations (Ro et al., 1999; Osan et al., 2000; Szaloki et al., 2000).

3. Results and discussion

3.1. Chemical composition of inhalable WF particle fractions (PM_1, $PM_{2.5}$, PM_{10})

The composition of the electrode coating determines the elemental composition, the formation intensity of PM_{10}, and the changes in composition with increasing heat input. Under identical experimental conditions, welding with an electrode with ilmenite coating (ANO-4i) instead of rutile (ANO-4) leads to an increased Fe and Mn content in PM_{10}. On the other hand, the insignificant ferromanganese content (5%) in the coatings of main type electrodes (UONI13/45) results in a relatively low contribution of manganese (Table 1).

An increased heat input causes an elevated temperature at the electrode tip, thereby intensifying the evaporation process and the formation rate of coarse fume particles (microspatter). These coarse particles contribute considerably to the total mass of the WF, since they are much larger compared to the fume particles formed through evaporation. The lowest fume formation rate was observed for ANO-4, and for UONI 13/45 it was the highest (Table 1).

Although an increase of the heat input is accompanied by an increased PM_{10} formation rate (from about 1.45–1.6 times), the elemental composition for this fraction varies only between 5% and 20%). The fume formation rate for PM_1, $PM_{2.5}$ and PM_{10} differed significantly, and represented about 67, 80, and 97% of the total mass, respectively (Fig. 2). Despite this significant difference in the fume formation rate, the elemental composition of these WF fractions was almost identical (Table 1).

Table 1
The elemental composition of PM_1, $PM_{2.5}$, and PM_{10} fractions and effect of heat input on the elemental composition of PM_{10}.

	Electrode type											
	UONI 13/45				ANO-4				ANO-4i			
	High heat input[a]			Low heat input[a]	High heat input[a]			Low heat input[a]	High heat input[a]			Low heat input[a]
	PM_1	$PM_{2.5}$	PM_{10}	PM_{10}	PM_1	$PM_{2.5}$	PM_{10}	PM_{10}	PM_1	$PM_{2.5}$	PM_{10}	PM_{10}
FFR[b] (g min^{-1})	0.64	0.80	0.93	0.59	0.56	0.71	0.82	0.53	0.61	0.76	0.87	0.6
Major elements (mass%)												
Fe	21.8	21.5	21.9	25.5	37.1	36.2	36.4	34.1	40.5	39.4	39.6	41.7
Mn	5.4	5.3	5.4	5.6	6.9	6.7	6.7	6.1	8.7	9.9	9.8	10.8
Ti	0.1	0.1	0.1	0.1	0.8	0.8	0.8	0.6	0.3	0.3	0.4	0.3
Ca	12.8	12.8	12.7	10.3	n.a.	n.a.	n.a.	n.a.	0.2	0.2	0.3	0.4
K	6.7	6.5	6.5	7.1	6.3	6.0	6.0	6.1	3.6	4.8	4.8	5.7
Si	3.6	3.4	3.6	3.2	9.2	8.7	8.8	7.8	7.9	9.7	9.5	8.3
Al	0.5	0.5	0.5	0.6	0.5	0.6	0.6	0.5	0.3	0.4	0.5	0.5
Trace elements[c]	0.9	0.9	0.8	0.9	1.1	1.0	1.0	1.0	1.1	1.0	1.0	0.9
Missing elements[d]	48.2	49.0	48.5	46.7	38.1	40.0	39.7	43.8	37.4	34.3	34.1	31.4

n.a.—Not available for detection because of element's low amount.
[a] Heat input: 1.36 kJ mm^{-1}.
[b] Fume Formation Rate.
[c] Cr, Ni, Cu, Zn, Pb, Cl, and S.
[d] Expected from electrode coating and oxidation: C, O, F, Na, Mg.

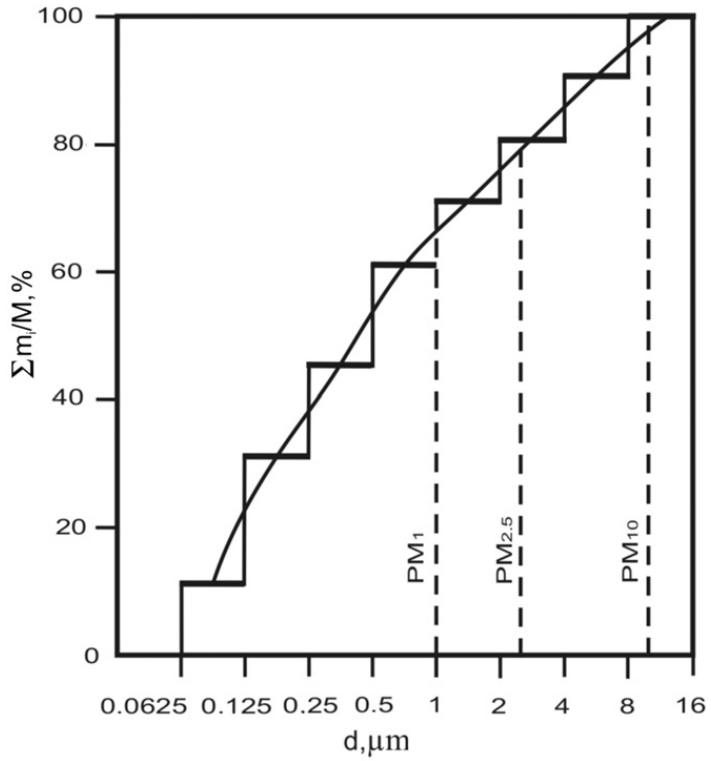

Fig. 2. Histogram of the WF mass distribution as a function of particle aerodynamic diameter. Welding conditions: UONI 13/45 electrode; 1.36 kJ mm^{-1}.

The results show that the classification of WF particles into fractions with a different degree of precipitation in the respiratory system (PM_1, $PM_{2.5}$, and PM_{10}) does not allow to examine the relationship between welding conditions, the elemental composition, and particle size. With such an approach, it is only possible to make a comparative hygienic evaluation of different types of welding materials, and to determine the fume formation rate of $PM_{2.5}$. The latter could be of special interest, since it directly characterizes the amount of WF precipitated in the human lung, and could be used for the development of air exchange requirements in the industrial space.

3.2. Chemical composition of individual WF particles

Since the analysis of the elemental composition of a particle with EPMA is semi-quantitative (Spolnik et al., 2005), only major relations between the elemental composition of WF particles and their aerodynamic size were identified.

Iron was chosen as the main element in the WF, and collected particles were divided into three groups according to their iron content: (1) low: less than 20%, (2) average: from 20 to 40%, and (3) high: more than 40%. The contribution of these groups to the six collected WF fractions for ANO-4 and UONI 13/45 electrodes are presented in Fig. 3.

Only slight differences were observed between the elemental compositions of particles with an average content of iron within the 0.25 to 16 μm EAD range (less than 25–30%). They are mainly represented by agglomerates (chains, clusters) of ultra-fine particles with various shapes and densities (Fig. 4). Insignificant differences in the composition of these agglomerates (which consist of multiple ultra-fine particles formed by vapor condensation) apparently reflect the variation of vapor composition in different regions of the welding torch. Maximum linear sizes of the agglomerates are 20–25 μm, but their aerodynamic size is less than 8–16 μm due to their low packing density. Particles with an average content of iron were the most abundant group (over 70%) of inhalable particles in the WF. Their average composition could be summarized as shown in Table 2 (mass%).

This composition heavily depends on the agglomerate size, since it is averaged over numerous ultra-fine particles, but it does not depend on the welding conditions. This can be explained by two competing processes, which occur when vapor enters the condensation zone of the welding torch: (1) evaporation from the electrode tip, and (2) condensation of vapors from the electrode material in the welding pool. In other words, the composition and amount of vapor in the condensation zone depends only on the part which does not condensate in the welding pool and is dispersed in the environment. The gas flow in the arc provides a carry-over of vapor from the electrode tip to the welded metal. An increase in heat input will increase the temperature at the tip of the electrode (in the active spot it can reach the boiling point of the electrode metal (Voitkevich, 1995), thereby elevating the intensity of electrode–material evaporation. Since the average temperature of the molten welding pool is only 100–200 K higher than the melting point of the mild steel weld plates (Yerokhin, 1973), condensation of vapors in the welding pool will take place along the gas-vapor flow, which spreads radially. Although the molten pool increases with heat input, its average temperature will remain almost the same. Moreover, when the

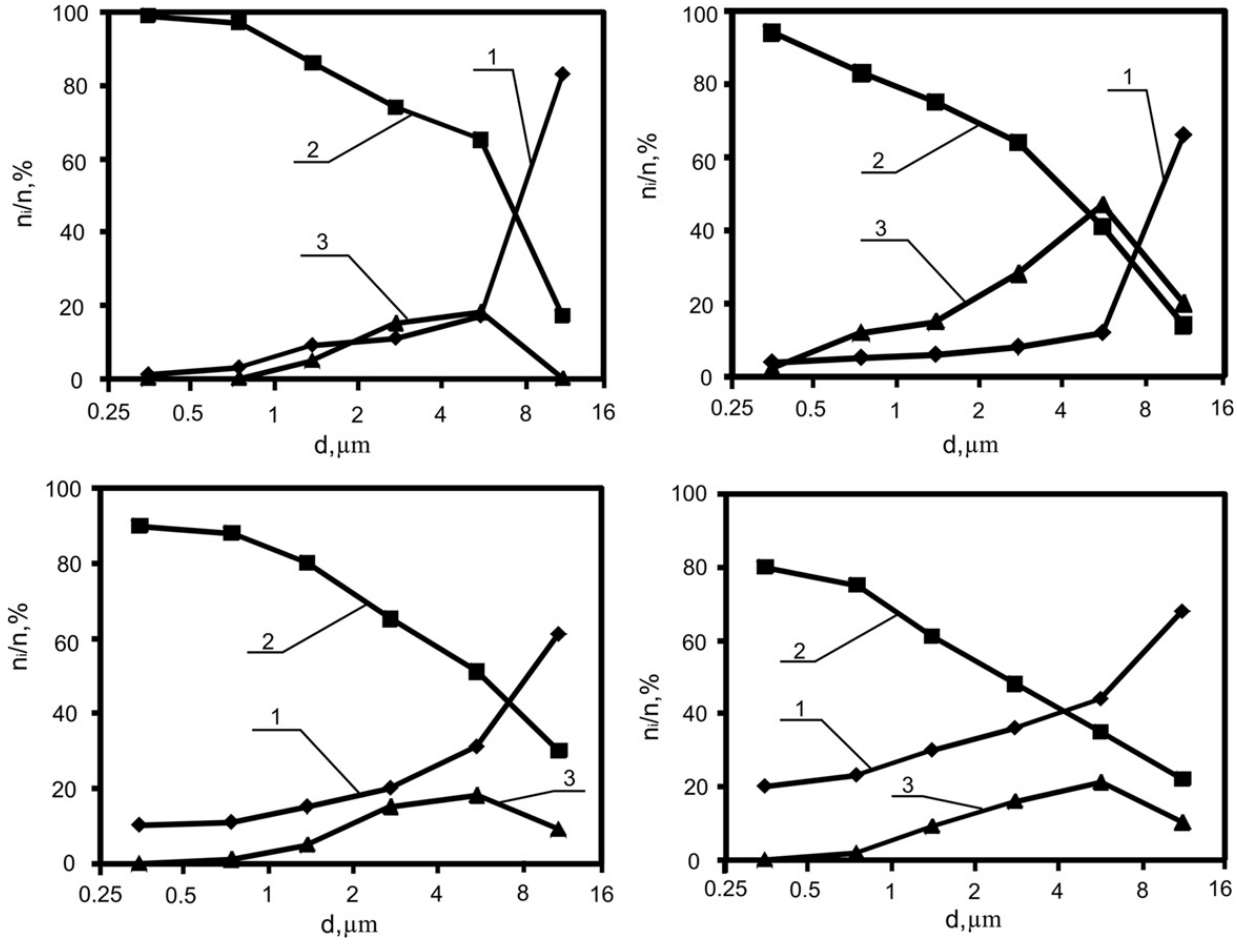

Fig. 3. Percentage of WF particles with a (1) low, (2) average, and (3) high content of iron as a function of aerodynamic size (EAD) – Top: ANO-4; Bottom: UONI 13/45; Left: 1 kJ mm^{-1}; Right: 1.36 kJ mm^{-1}.

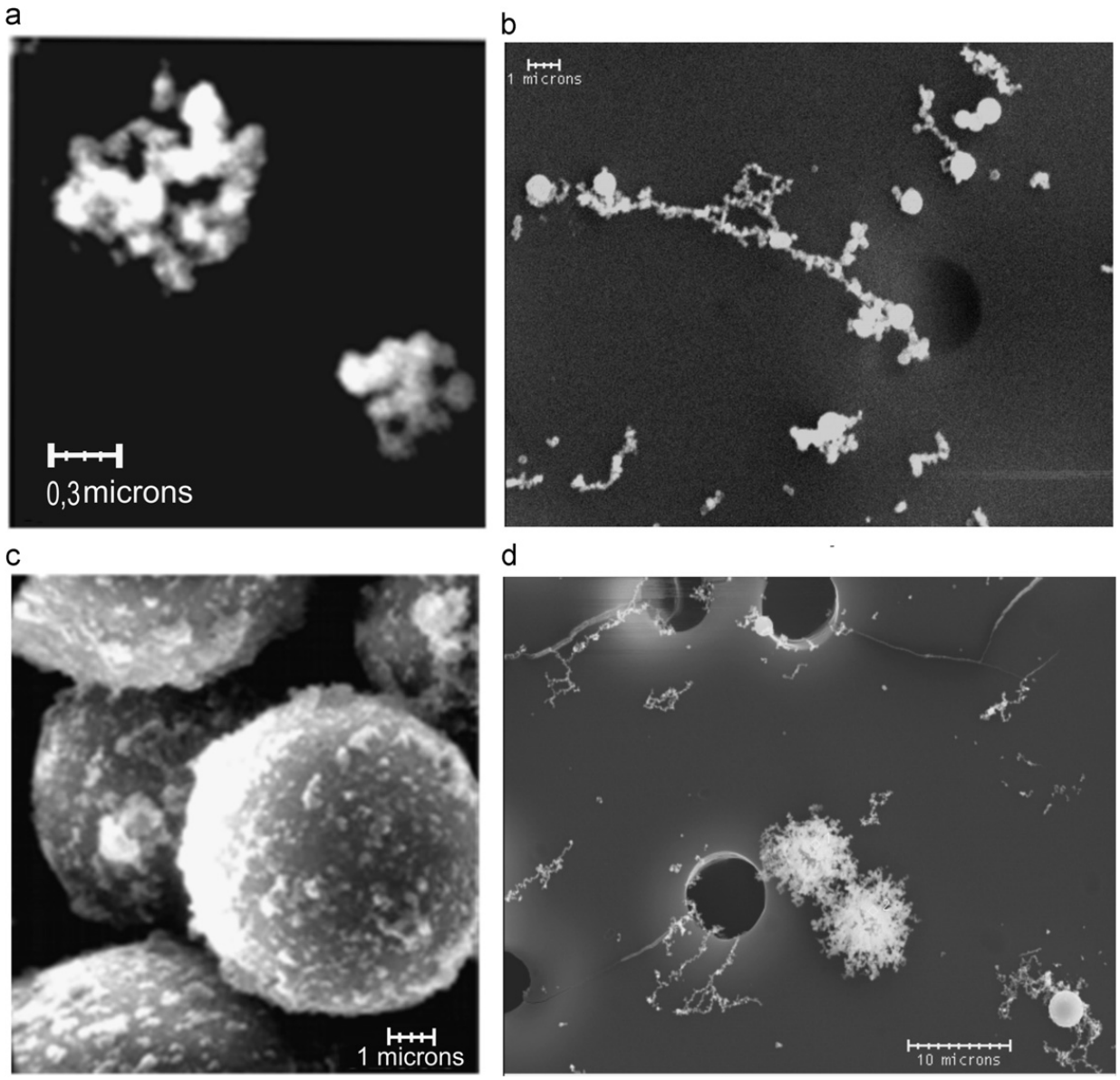

Fig. 4. Aggregates of ultra-fine particles with various shapes and densities (a) clusters, (b) chains, (c) spherical particles with a smooth surface on which ultra-fine particles are located, (d) aggregates of particles covered by ultra-fine particles and arose from the disintegration. Images of the WF particles obtained with scanning electron microscope coupled with energy dispersive X-Ray detector (SEM/EDX, JEOL 6300, Japan).

Table 2
Average composition of elements typical of group 2 for different welding electrodes applied. Results got by Voitkevich et al. (1984) are added in brackets.

Electrode type	Elements (mass%)											
	Fe	Mn	Ti	Ca	K	Si	Al	Mg	Na	O	C	F
ANO-4	34 (37)	8.2 (7.2)	1.9 (0.9)	n.a. (n.a.)	3.5 (8.9)	8.6 (8.0)	1.6 (n.a.)	2.2 (0.5)	2.3 (3.0)	28.1 (32.9)	6.1 –	n.a. (1.2)
UONI-13/45	28.7 (20.8)	5.7 (5.5)	n.a. (0.2)	4.4 (14.1)	n.a. (2.1)	5.2 (2.8)	1.6 (n.a.)	1.1 (n.a.)	3.9 (14.7)	24.3 (23.7)	10.1 –	12.5 (14.4)

n.a.—Not available for detection because element's amount is too low.

mechanical effects of flow increase with heat input, and the liquid metal is pushed out of the arc significantly, pool temperature can even decrease due to the intensification of heat sink conditions and convection in the pool (Yerokhin, 1973). This results in a larger surface area in which the generated multi-component vapor could condense, thereby reducing variations of the elemental composition of the vapor produced on the electrode tip. Since both processes are in equilibrium, only a slight dependence can be observed between the composition of vapor entering the condensation zone of the welding torch and the applied heat input.

Particles with a low content of iron (group 1) are rich in C, O, and elements from the electrode coating (e.g. Na, Mg, Al, Si, K, and Ti for ANO-4 electrodes, and additionally Ca and F for UONI 13/45 electrodes). These particles could be identified as agglomerates of ultra-fine particles, and particles formed by disintegration of the electrode-coating (Fig. 4). Disintegration (or spray) of the electrode-coating is caused by intense gas emissions due to (i) carbonate thermolysis, (ii) cellulose pyrolysis, and (iii) CaF_2 pyrohydrolysis. Additionally, the slag draining directly into the welding pool also promotes the spraying effects (Yerokhin, 1973).

WF particles with a high content of iron (group 3) are formed by the spray of electrode metal droplets coated by layer of molten slag. These smooth spherical particles are rich in iron (40–80%) and oxygen (19–25%), and are covered by numerous ultra-fine particles (Fig. 4). Particles with high Fe-content are most abundant in the WF fraction with EAD from 4 to 8 μm.

Two processes are responsible for the ejection of electrode-metal particles of micrometer size: (1) local explosive gas emissions in the volume of the metal (caused by metallurgical reactions), resulting in the release of metal particles from the electrode-droplet, or, in a rare occasion, from the welding pool; and (2) explosive destruction of the electrode-droplet bridge due to an acute increased current density (Yerokhin, 1973).

The spray of these iron-rich particles is mainly affected by the heat input and the composition of the electrode coatings. For rutile-coated electrodes (ANO-4), an increase of the heat input results in a visible increase of WF particles with a high content of iron, and expands their EAD size range (Fig. 3). The opposite trend is observed for electrodes with a carbonate–fluorite coating (UONI 13/45): the portion of WF particles with a low content of iron in the range of 0.25–8.0 μm EAD is almost doubled when elevating the heat input (Fig. 3).

These trends explain why the content of iron in PM_{10} for UONI 13/45 electrodes decreases with increasing heat input, while for ANO-4 electrodes an increase was observed (Table 1). Noteworthy, due to the physical and chemical properties of the electrode coating, ANO-4 electrodes are characterized by smaller metal-droplet transfers from the molten electrode-metal to the welding pool, as compared to UONI 13/45 electrodes (Pokhodnya et al., 2004).

The comparison of results (Tables 1 and 2) demonstrates that bulk elemental composition of WF (Voitkevich et al., 1984) as well as fractions PM_1, $PM_{2.5}$, PM_{10} do not present detail elemental composition of ultrafine particles agglomerates which are the most toxic fraction because of their large specific surface. Therefore it is important to extract that group of particles and analyze them separately.

4. Conclusions

The obtained results on the composition of WF particles (0.25–16 μm EAD) formed during SMAW suggest simultaneous formation of three WF particle types in the welder's breathing zone. Each type contains various amounts of elements originating from the welding materials, which reflect their mechanism of formation. Particles could be classified into three groups corresponding to low—($< 20\%$), average—(20–40%) and high—($> 40\%$) content of iron.

For each electrode type the abundance of these particle types in the WF depends on the heat input during welding.

The small differences in the elemental composition of inhalable particle fractions (PM_1, $PM_{2.5}$, and PM_{10}) result from averaging the composition over the three particle groups (according to their shares) within the corresponding size range. More intense disintegration processes (microspatter formation) of the welding materials accounted for the lack of correlation between elemental composition of PM_{10} and heat input (changes within 5–20%).

Particles with an average content of iron (agglomerates of ultra-fine particles) formed the largest group (over 70%) of inhaled particles in the WF. For each electrode type, their average elemental composition did not depend either on the size of the agglomerates, or on the heat input.

The obtained results could be useful for sanitary-hygienic assessments of welding consumables and conditions.

References

Hewett, P. (1995). Estimation of regional pulmonary deposition and exposure for fFumes from SMAW and GMAW mild and stainless steel consumables. *American Industrial Hygiene Association Journal*, *56*, 136–142.

Holsapple, M.P., Farland, W.H., Landry, T.D., Monteiro-Riviere, N.A., Carter, J.M., Walker, N.J., & Thomas, K.V. (2005). Research strategies for safety evaluation of nanomaterials, part II: toxicological and safety evaluation of nanomaterials, current challenges and data needs. *Toxicological Sciences*, *88*, 12–17.

International Standards Organization. (2002). *Health and Safety in Welding and Allied Processes—Laboratory Method for Sampling Fume and Gases Generated by Arc Welding—Part 1: Determination of Emission Rate and Sampling for Analysis of Particulate Fume*. ISO: Geneva EN ISO 15011-1:2002.

Jenkins, N.T., Pierce, W.M.G., & Eagar, T.W. (2005). Particle size distribution of gas metal and flux cored arc welding fumes. *Welding Journal*, *84*, 156–163.

Lioy, P.J., Wainman, T., Turner, W., & Marple, V.A. (1988). An intercomparison of the indoor air sampling impactor and the dichotomous sampler for a 10 μm cut size. International. *Journal of Air Pollution Control and Hazardous Waste Management*, *38*, 668–670.

Marple, V.A., Rubow, K.L., Turner, W., & Spengler, J.D. (1987). Low flow-rate sharp cut impactors for indoor air sampling—design and calibration. *International Journal of Air Pollution Control and Hazardous Waste Management*, *37*, 1303–1307.

Osan, J., Szaloki, I., Ro, C.-U., & Van Grieken, R. (2000). Light element analysis of individual microparticles using thin-window EPMA. *Mikrochimica Acta*, *132*, 349–355.

Pokhodnya, I.K., Yavdoshchin, I.R., & Paltsevich, A.P. (2004). *Metallurgy of Arc Welding: Interaction of Metal with Gases*. Naukova dumka: Kiev.

Ro, C.U., Osan, J., & Van Grieken, R. (1999). Determination of low-Z elements in individual environmental particles using windowless EPMA. *Analytical Chemistry*, *71*, 1521–1528.

Sowards, J.W., Lippold, J.C., Dickinson, D.W., & Ramirez, A.J. (2008). Characterization of welding fume from SMAW electrodes. *Welding Journal: Welding Research*, *87*, 106–112.

Spolnik, Z., Belikov, K., Van Meel, K., Adriaenssens, E., De Roeck, F., & Van Grieken, R. (2005). Optimization of measurement conditions of an energy dispersive X-ray fluorescence spectrometer with high-energy polarized beam excitation for analysis of aerosol filters. *Applied Spectroscopy*, *59*, 1465–1469.

Szaloki, I., Osan, J., Ro, C.U., & Van Grieken, R. (2000). Quantitative characterization of individual aerosol particles by thin-window electron probe microanalysis combined with iterative simulation. *Spectrochimica Acta Part B-Atomic Spectroscopy*, *55*, 1017–1030.

Szalóki, I., Osán, J., Worobiec, A., de Hoog, J., & Van Grieken, R. (2001). Optimization of experimental conditions of thin-window EPMA for light-element analysis of individual environmental particles. *X-Ray Spectrometry*, *30*, 143–155.

Vekemans, B., Janssens, K., Vincze, L., Adams, F., & Van Espen, P. (1994). Analysis of x-ray spectra by iterative least squares (AXIL): new developments. *X-Ray Spectrometry*, *23*, 278–285.

Voitkevich, V.G. (1982). Methods for studying welding fumes. *The Paton Welding Journal*, *3*, 51–54.

Voitkevich, V.G., Bezruk, L.I., & Esaulenko, G.B. (1984). Investigation of welding fume by electron microscopy method. *The Paton Welding Journal*, *6*, 33–35.

Voitkevich, V.G. (1995). *Welding Fumes Formation, Properties and Biological Effects*. Abington Publishing: Cambridge.

Worobiec, A., Stefaniak, E.A., Kiro, S., Oprya, M., Bekshaev, A., Spolnik, Z., Potgieter-Vermaak, S.S., Ennan, A., & Van Grieken, R. (2007). Comprehensive microanalytical study of welding aerosols with X-ray and Raman based methods. *X-Ray Spectrometry*, *36*, 328–335.

Yerokhin, A.A. (1973). *Fundamentals of fusion welding*. Mashinostroenie: Moscow.

Zimmer, A.T., & Biswas, P. (2001). Characterization of the aerosols resulting from arc welding processes. *Journal of Aerosol Science*, *32*, 993–1008.